Segmentation of pelvic structures from planning CT based on a statistical shape model with a multiscale edge detector and geometrical likelihood measures

Fabio Martinez[1,2,4], Oscar Acosta[1,2], Gaël Dréan[1,2], Antoine Simon[1,2], Pascal Haigron[1,2], Renaud de Crevoisier[1,2,3], and Eduardo Romero[4]

[1] INSERM, U 1099, Rennes, F-35000, France
[2] Université de Rennes 1, LTSI, F-35000, France
{Oscar.Acosta, Gael.Drean, Antoine.Simon, Pascal.Haigron}@univ-rennes1.fr
[3] Département de Radiothérapie, Centre Eugène Marquis, Rennes, F-35000, France
r.de-crevoisier@rennes.unicancer.fr
[4] CIM&Lab, Universidad Nacional de Colombia, Bogota, Colombia
{edromero, fmartinezc}@unal.edu.co

Abstract. Accurate segmentation of the prostate and the organs at risk in CT images is a crucial step in prostate cancer radiotherapy planning. Because of the poor soft tissue CT contrast (prostate, bladder), an appropriate segmentation is challenging, even when this is manually performed by an expert. This paper introduces a Bayesian automatic segmentation method for prostate, rectum and bladder in planning CT. Firstly, a prior shape space for the organs is built with PCA decomposition from a population of manually delineated CT images. Then, for a given CT to be segmented, the most similar shape is selected by the associated probability which is set by a likelihood function. Finally, the local shape is deformed to adjust the particular local edges of each organ such that the most likely segmentation is produced. Experiments with real data from 30 patients treated for prostate cancer radiotherapy were performed under a leave-one out cross validation scheme. Results show that the method produces reliable segmentations (Averaged Dice = 0.91 for prostate, 0.94 for bladder, 0.89 for Rectum) and outperforms the best majority-vote multi-atlas based approach.

1 Introduction

Prostate cancer (PC) is one of the most commonly diagnosed male cancer, with 190.000 new cases diagnosed in USA in 2010 (American Cancer Society) and 71.000 new cases in France in 2011 (INCa 2011). Radiation therapy is a commonly prescribed treatment for PC which has proven to be efficient for tumor control [1]. Modern prostate cancer radiotherapy involves an extensive use of X-ray imaging modalities: a computed tomography (CT) acquisition in the treatment planning and daily cone beam CT (CBCT) in image-guided radiotherapy procedures (IGRT). During the planning, CT images are manually processed to segment not only the clinical target (prostate and seminal vesicles) but also the neighboring organs at risks (OARs), namely the bladder, rectum, etc. These segmentations are crucial inputs for the treatment planning in order to compute the parameters for the accelerators following dose constraints to the target and OARs, and, considering IGRT, for the patient setup correction. Moreover, these segmentations

are up the most importance for other applications like the cumulated dose computation or toxicity studies on population [3].

Nowadays, the segmentations are manually carried out by medical experts. They are very time consuming and are prone to errors due to intra- and inter-experts variability. Thus, the need for automatic segmentation methods appears crucial for IGRT development. However, several difficulties arise and hamper automatic segmentation methods. The poor contrast appearing in similar soft tissues, has limited application of classical intensity-based methods, while the very high intra- and inter-individual variability has led model-based methods to fail. Some examples of previous methods to segment pelvic structures include deformable models [5,6]. Atlas-based segmentations [7] have also been used, but they have mainly been tested for segmenting CT scans in other applications such as head and neck [8] and cardiac aortic CT [9]. In atlas based approaches, precomputed segmentations in a template space are mapped to an individual CT using non-rigid registration. Although atlas-based approaches may provide prior structural information, the inter-individual variability and registration errors can mislead these methods. Multi-atlas approaches can partly overcome some of these difficulties by selecting the most similar atlases among a large database but the definition of a proper similarity measure between the available atlases and the query individual has still to be addressed [10].

We propose in this paper a method to segment pelvic structures from CT scans to be used in planning prostate cancer radiotherapy. The main contribution of this work is the adaptation of a Bayesian statistical framework to match a prior 3D shape model, built from a population, with the given CT through multi-scale edge observations. Regions of Interest (RoI's) are automatically extracted per slice to remove CT artifacts and compute the multiscale edge descriptor. The likelihood function is based on a geometrical shape characterization of edges using invariant Hu moments, allowing the selection of the most likely prior 3D shape to the multi-scale detected edges. In a final step, the obtained shape is locally warped to fit to the edges, yielding a 3D regular and compact organ segmentation. We compared our method with majority-vote multi-atlas strategies in a leave-one-out cross validation scheme.

2 Materials and Methods

The overall method is summarized in Figure 1. Let $\widehat{S_o}$, the estimated organ shape (prostate, bladder or rectum), computed as the most likely shape that maximizes the maximum a posteriori (MAP), following a Bayesian framework

$$\widehat{S_o} = \max_{\widehat{S_o}} \arg[P(\widehat{S_o}|S^{pca}_{o_1}, S^{pca}_{o_2}, \ldots, S^{pca}_{o_N})]$$

where $\{S^{pca}_{o_1}, S^{pca}_{o_2}, \ldots, S^{pca}_{o_N}\}$ is a collection of shapes (shape space) of the organ o precomputed with a Principal component analysis (PCA). The likelihood function aims to match the most similar shape to the borders extracted from a region of interest (RoI) automatically selected around the organ o. In order to remove CT artifacts, a pre-processing procedure is applied over the RoI. Afterward, a local deformation function is introduced to modify the most probable estimated shapes $\widehat{S_o}$, according to the local changes extracted from a multiscale edge descriptor. Each step is described in the following sections.

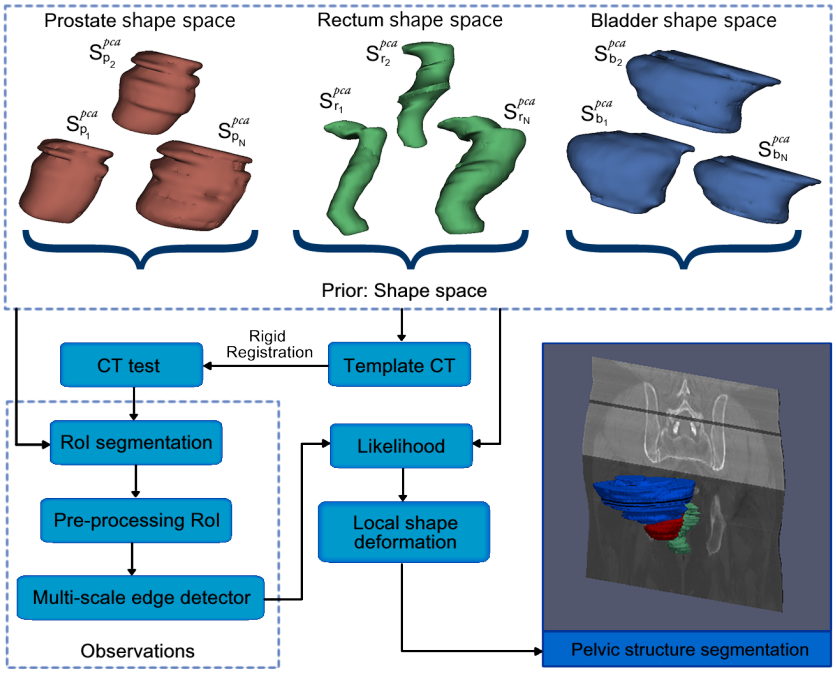

Fig. 1. Proposed method for 3D segmentation. First, a shape space organs is built (PCA). The template is rigidly registered to the CT to be segmented followed by an automatic extraction of RoIs for preprocessing and multi-scale edge detection. A likelihood function matches the most similar PCA shape with the detected edges to finally being locally adjusted.

2.1 Learning an organ shape model: the prior

A statistical shape organ model for segmentation is built from a collection of training samples as described in [11]. Here, a dimensionality reduction was firstly accomplished by applying the PCA method [12] to a population of manually delineated organs encoding interindividual shape variability [13]. From this PCA was computed the collection of shapes $\{S^{pca}_{o_1}, S^{pca}_{o_2}, \ldots, S^{pca}_{o_N}\}$, for each considered organ. Each shape contour is the parametric curve defined by the coordinates of the points lying on the contour. The first step consisted then in computing the first two moments of the probability distribution, i.e. the mean shape vector $\bar{s} \in R^{3M}$ and the covariance matrix $\rho \in R^{3Mx3M}$, as $\bar{s} = \frac{1}{N}\sum_{i=1}^{n} s_i$ and $\rho = \frac{1}{N-1}\sum_{i=1}^{n}(s_i - \bar{s})(s_i - \bar{s})^T$ where the vector $(s_i - \bar{s})$ describes the organ deviation w.r.t. the mean shape. The covariance matrix captures the organ variability. A conventional spectral analysis allows diagonalization of this covariance matrix that determines the directional gains or *eigenmodes*. Each eigenmode defines a 3D vector field of correlated organ inter patient-variability displacements. Thus, prostate and OAR samples are generated by deforming the mean shape by a weighted sum of the L dominating eigenmodes as:

$$S_{o_l}^{pca} = \bar{s} + \sum_{l=1}^{L} c_l q_l$$

where the coefficients of c_l follow a Gaussian distribution with the corresponding eigenvalues q_l as variances. This methodology was independently used for each organ, obtaining a family of shape models that are related with a template CT global coordinates. Examples of the different shapes obtained for each organ are shown in Figure 1.

2.2 RoI pre-processing

For a given CT, it is firstly rigidly registered with the template CT of the training database using a "block matching" method [14]. Over CT test is then defined a set of RoIs with size $\{\bar{S}_o \pm \xi\}$ associated to each organ, being $\bar{S}_o$ the average shape and ξ a tolerance value. An theoretical ideal $RoI_o(x, y)$ should contain the foreground organ of interest and a uniform background distribution, a particular configuration herein modeled as a mixture of Gaussians $\psi(i) = \sum_{k=1,2} w_k N(i|\mu_k, \sigma_k^2)$, where the two principal distributions represent the foreground and background, weighted by w_k. Because very often the selected RoIs contain other structures near the organs, difficulting a proper edge extraction of the organ and therefore biasing the statistical approximation, a more appropriate representation is found by filtering out RoI with an adapted non local mean. Thus, pixels i that may represent artifacts $\{i < \max_{k=1,2}(2\sigma_k) < i\}$ are replaced by a weighted average of a neighborhood with foreground/background information, thereby, satisfying a "non local property": weights depend on the pixel similarity in the image space, $\varrho(x, y) = e^{\frac{-d(x,y)}{h^2}}$. The basic idea is to replace the pixels that represent artifacts by the nearest "foreground/background" pixel that represent the neighborhood. $d(x, y) = \sum_{i \in \phi(o)} \left\| RoI_o(x, y) - N_{k1,k2}(\mu, \sigma^2) \right\|$, where $\phi(o)$ is a neighborhood of x an h is a decay parameter.

2.3 Multi-scale CT edge detector: the observations

To build a set of robust observations to be used within the likelihood function a multiscale description of RoI data was implemented. For doing so, each $RoI_o(x, y)$ was convolved several times with a gaussian kernel and first partial derivatives were calculated at the different resolution scales as:

$$S_o^{edge}(x, y; \sigma) = \sum_i RoI_o(x, y) * \frac{\partial G_{\sigma_i}}{\partial_x \partial_y}$$

where G_{σ_i} is the 2D Gaussian function with standard deviation σ_i. The Gaussian kernel is the unique kernel with an equivalent scale-space representation (linearity and shift-invariance in both frequency and space). Afterward, a non-maximum suppression is applied, aiming to detect points at which the gradient magnitude takes a maximum value in the gradient direction over all the scales [15]. This multi-scale edge detection allows a compact description of the most relevant information which is usually preserved through multiple scales (*the universal law of scale invariance*) [16].

2.4 Computing the likelihood

A likelihood function $P(\widehat{S}_{o_j}^{pca}|S_o^{edge})$ determines the best geometrical match between the samples shapes $\widehat{S}_{o_j}^{pca}$ obtained from the learned model and each multi scale edge descriptor S_o^{edge}. For doing so, every shape from the shape space and the edges in each RoI are characterized by a set of features based on the Hu moments [2], thereby achieving an invariant shape representation. Thus the likelihood function measures the shape similarity through an Euclidean metric among the computed features, written as:

$$P(S_{o_i}^{PCA}|S_{o_i}^{edge}) = \min_{S_{o_j}^{pca}} \left\{ \sum_{h_u(i=1...7)} \frac{||m_i^{S_o^{edge}} - m_i^{S_{o_j}^{pca}}||}{m_i^{S_o^{edge}}} \right\}$$

where $m_i^{S_o^{edge}} = sign(h_i^{S_o^{edge}}) \cdot \log|h_i^{S_o^{edge}}|$, and $m_i^{S_{o_j}^{pca}} = sign(h_i^{S_{o_j}^{pca}}) \cdot \log|h_i^{S_{o_j}^{pca}}|$ are the computed features for the edges and the PCA learned shapes respectively and $h_i^{S^{edge}}$, $h_i^{S_j^{pca}}$ are the Hu moments. Then, the likelihood function should yield a maximal probability when a sample learned shape closely match the observations, i.e., the multiscale edge descriptor.

2.5 Local Shape Deformation

A local deformation function was here introduced to improve the local correspondence of the shape sample selected by the PCA model with respect to near shape edges detected and allows to regularize the segmentation surface obtained. For doing this, the nearest borders that may correspond to the edges of the multiscale descriptor or the borders points of the shape sagittal estimation. Then the edges were warped toward the nearest border, controlling the deformation by a λ term, which works as a belief indicator warping the shape either to the border descriptor or to the PCA shape selected.

$$So_i(x,y) = \lambda \widehat{S}_{o_i}^{pca}(x,y) + (1-\lambda)(\min_{S_o}(\|\widehat{S}_{o_i}^{pca} - \{S_{o_i}^{edge}, \widehat{S}_{o_{i\pm1}}^{pca}\}\|))$$

This local deformation allows to preserve a compact representation of the shape given by the λ term and the nearest edge criterion. In this work, the best performance was obtained with a $\lambda = 0.6$

3 Evaluation and Results

We carried out a study on 30 prostate cancer patients, treated with external radiotherapy. Each individual underwent a planning CT. All acquired CT were 2 mm thickness slice with a 512x512x1 mm-pixels resolution in the axial plan. For each individual, the organs were manually delineated by the same expert, following the standard clinical protocol in prostate cancer radiotherapy. The expert contoured the clinical targets - namely the prostate and the seminal vesicles - and the organs at risk (OAR): the bladder and the rectum. In this study, only the CT and the delineated prostate, bladder and rectum were considered.

We aimed to compare individual's radiologist segmentations (ground truth) with the obtained by the proposed approach and those obtained with multi-atlas vote methods, on a set of 30 individuals, following a leave-one-out cross validation scheme. The

multi-atlas vote methods, used to evaluate the performance of the proposed approach, may be summarized in three main step. Firstly, the atlases rigidly registered using a "block matching" strategy were ranked according to the normalized cross-correlation (NCC) [14]. Secondly, the organs delineations were propagated into the individual's space, using a non-rigid registration, either the free-form deformation (FFD) [17], or the demons algorithm [18]. Eventually, the majority vote decision rule was applied to obtained a single segmentation for each considered organs.

Figure 2 illustrates a typical pelvic structures segmentation obtained by our approach (red contour) and the the radiologist reference represented by the green contour. These results shows the effectiveness obtained by our approach to closely adjust each organ structure. Likewise, it is shown a good local variability shape which preserve a compact representation, which means that, there are no strong spikes around the contour shapes.

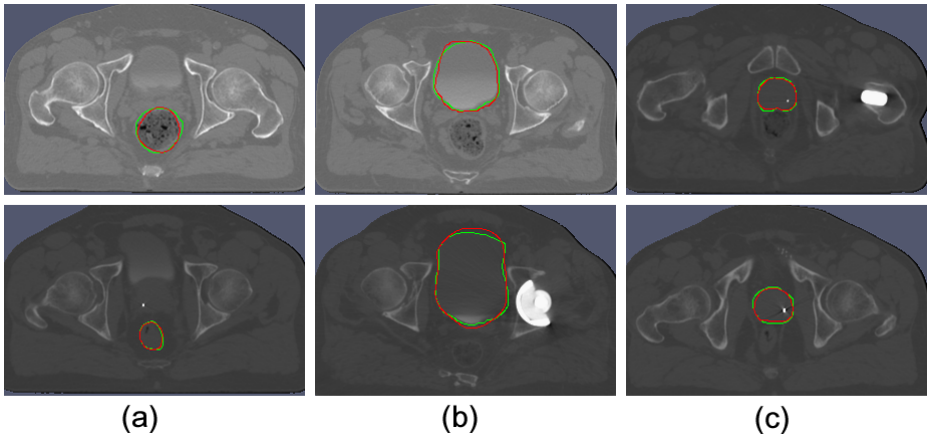

Fig. 2. Axial segmentation examples of pelvic structures ((a) rectum, (b) bladder and (c) prostate). The delineation obtained by our approach (red) and the expert reference (green).

A quantitative comparison was performed between the individual's organ delineations (prostate, bladder, rectum) and the computed segmentation using two different measures: a dice score (DSC) and the Hausdorff distance.

The DSC is an overlapping similarity measure defined as $DSC(A,B) = \frac{2|A \cap B|}{|A|+|B|}$, where $|\cdot|$ indicates the number of voxels of the considered A (gold standard) and B (method evaluated) volumes. We carried out an exploratory analysis of DSC obtained with the different segmentation strategies. Figure 3 illustrates the results comparing our approach with the atlas based methods. Results suggest that our method provide more accurate segmentations (t-test,$p<0.001$ for the prostate and the rectum) with an average score of 0.91 for prostate, 0.94 for bladder, 0.89 for Rectum

A second quantitative comparison was performed by computing the Hausdorff Distance. This metric identifies the segmentation voxel that is farthest from any voxel of the ground truth. Table 1 summarizes the performance obtained by the evaluated ap-

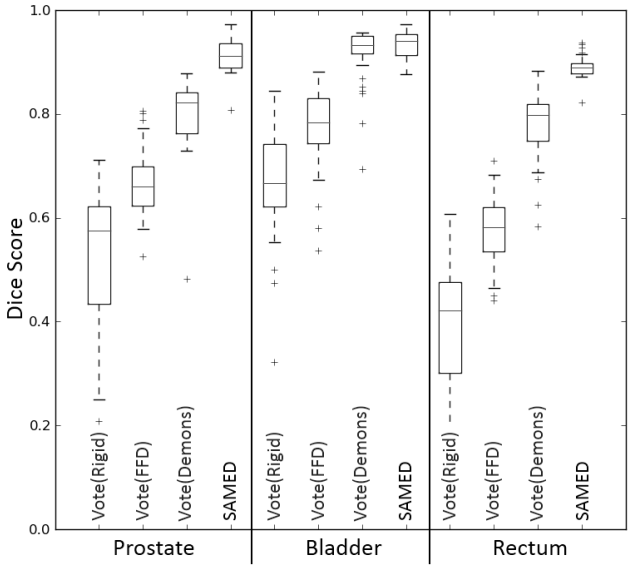

Fig. 3. Dice scores comparison for vote vs proposed approach (SAMED)

Table 1. The Hausdorff distances obtained with the multi-atlas majority-vote method using rigid, FFD or a demons registration and with the proposed approach (SAMED)

	Hausdorff Distance (mm)		
	Prostate	Bladder	Rectum
Vote(Rigid)	16.61±5.6	102.02±26	66.87±10.3
Vote(FFD)	14.27±4.2	78.63±20.1	65.22±6.1
Vote(Demons)	9.33±3.2	79.42±18.2	61.44±5.8
SAMED	5.98±2.2	19.09±3.1	7.52±2.3

proaches. The results shows that our approach obtain compact shape segmentations, with average distances of 5.98 for the prostate, 19.09 for the bladder and 7.52 for the rectum. The large distance of the multi-atlas based methods may be attributed to isolated voxels labeled as organ structure.

4 Conclusions

The proposed method introduces a new methodology to segment pelvic structures in CT scans used in prostate cancer radiotherapy. The Bayesian method combines a deformable prostate model, learned by examples, and a geometrical likelihood strategy that maps this model into a particular CT image, adequately described by a multiscale edge detector. The results summarized in this paper pointed out that our segmentation technique segment the prostate and rectum shape suitably in relation to radiologists' reference. This approach also may be extended to other structures over CT images. Future work includes validation with a large data set.

Acknowledgements

This work is partially supported by Rennes Metropole through a mobility scholarship, the project ANR TIGRE and the Universidad Nacional de Colombia Ph.D scholarship.

References

1. D'Amico, *et al*: Biochemical outcome after radical prostatectomy, external beam radiation therapy, or interstitial radiation therapy for clinically localized prostate cancer. AMA **280** (1998)
2. D. Zhang: Review of shape representation and description techniques. Pattern Recognition, 37(1):1-19, 2004.
3. Heemsbergen, W.D., *et al*: Urinary obstruction in prostate cancer patients from the dutch trial (68 gy vs. 78 gy): Relationships with local dose, acute effects, and baseline characteristics. Int J Radiat Oncol Biol Phys (2010)
4. Acosta, O.,*et al*: Atlas based segmentation and mapping of organs at risk from planning CT for the development of voxel-wise predictive models of toxicity in prostate radiotherapy. In:Prostate Cancer Imaging. International Workshop in MICCAI 2010. LNCS 6367. 42–51. (2010)
5. Costa, M.J., *et al*: Automatic segmentation of bladder and prostate using coupled 3D deformable models. Med Image Comput Comput Assist Interv **10** (2007) 252–260
6. D. Bystrov, *et al*: Simultaneous fully automatic segmentation of male pelvic risk structures. In: Estro. European society for Radioherapy and oncology. (2012)
7. Rohlfing, *et al*: Multi-classifier framework for atlas-based image segmentation. Computer Vision and Pattern Recognition, IEEE Computer Society Conference on **1** (2004) 255–260
8. Han, X., Hoogeman, *et al*: Atlas-based auto-segmentation of head and neck CT images. (2008) 434–441
9. Isgum, I., *et al*: Multi-atlas-based segmentation with local decision fusion - application to cardiac and aortic segmentation in CT scans. IEEE Transactions on Medical Imaging **28** (2009) 1000–1010
10. Acosta, O., *et al*: Evaluation of multi-atlas-based segmentation of ct scans in prostate cancer radiotherapy. IEEE ISBI. (2011) 1966 –1969
11. Heimann, T., Meinzer, H.P.: Statistical shape models for 3d medical image segmentation: A review. Medical Image Analysis **13** (2009) 543 – 563
12. Sohn, M., *et al*: Modelling individual geometric variation based on dominant eigenmodes of organ deformation: implementation and evaluation. Physics in Medicine and Biology **50** (2005) 5893
13. Lorenz, C.,*et al*: Generation of Point-Based 3D Statistical Shape Models for Anatomical Objects. CVIU **77** (2000) 175–191
14. Ourselin, S., *et al*: Reconstructing a 3D structure from serial histological sections. Image and Vision Computing **19** (2001) 25 – 31
15. Lindeberg, T.: Feature detection with automatic scale selection. Int. J. Comput. Vision **30** (1998) 79–116
16. Ter Haar Romeny,*et al*: Scale space: Its natural operators and differential invariants. In Colchester.: Information Processing in Medical Imaging. Springer Berlin / Heidelberg (1991) 239–255
17. Rueckert, D., *et al*: Nonrigid registration using free-form deformations: Application to breast mr images. IEEE Transactions on Medical Imaging **18** (1999) 712–721
18. Thirion, J.P.: Image matching as a diffusion process: an analogy with maxwell's demons. Medical Image Analysis **2** (1998) 243 – 260